Characterization of the mixed-mode interlaminar fracture toughness of an Additive Manufacturing continuous carbon fiber reinforced-thermoplastic composite

Jonnathan D. Santos [1], Sakineh Fotouhi[2], José M. Guerrero [3] and Norbert Blanco [3,*]

[1] Análisis y Tecnología de Estructuras en Ingeniería (ATEI), Universidad Politécnica Salesiana, Calle Vieja 12-30 y Elia Liut, Cuenca 010105, Ecuador.

[2] School of Engineering, University of the West of England, Frenchay Campus, Coldharbour Lane, Bristol BS16 1QY, United Kingdom.

[3] Analysis and Advanced Materials for Structural Design (AMADE), Department of Mechanical Engineering and Industrial Construction, Universitat de Girona, Avda. M. Aurèlia Capmany 61, 17003 Girona, Spain.

[*] Corresponding author. *E-mail address:* norbert.blanco@udg.edu (N. Blanco)

Abstract

There is a lack of knowledge concerning the interlaminar fracture toughness under mixed-mode ratios of 3D-printed composites. In this work, several Additive Manufacturing (AM) continuous Fiber Reinforced Thermoplastic (cFRT) specimens have been tested to characterize the initiation and propagation of interlaminar fracture toughness under three different mixed-mode $G_{II}/(G_I+G_{II})$ ratios: 25, 50 and 75%. The results obtained do not exhibit the common tendency seen in traditional laminated composite materials, in which the fracture toughness increases with the mixed-mode ratio. While the fracture toughness for the 50% mixed-mode ratio falls between the corresponding mode I and mode II values, the fracture toughness for the 25 and 75% ratios falls outside this range. To provide a reasonable explanation, fractography and microstructure analyses were conducted to quantify fiber, matrix and void contents. It was concluded that this uncommon behavior is probably related to the intrinsic variability of the material and manufacturing process.

Keywords: 3-D Printing; Fracture toughness; Mechanical testing; Mixed-mode fracture

Highlights:

- Continuous fibers improve mechanical properties of 3D-printed composite parts

- Delamination is a critical failure mode for laminated composite materials

- Characterization of mixed-mode delamination is key for simulation and design

- First complete study of mixed-mode delamination for 3D-printed composites

1. Introduction

Continuous Fiber-Reinforced Polymer (FRP) composites are widely employed in many industrial applications, such as aerospace, automotive, sport, energy industries, construction and defense, thanks to their excellent strength and stiffness to weight ratio. They are traditionally manufactured by means of Resin Transfer Molding, pultrusion, spray-up, Automated Fiber Placement and Filament Wilding, among others. These techniques require time-consuming tasks, in addition to expensive curing equipment and tooling, which are economically unsuitable for a limited batch of production. These drawbacks have prompted the increased utilization of Additive Manufacturing (AM), commonly referred to as 3D printing. This method has several advantages over traditional manufacturing: (i) it allows to manufacture complex geometry patterns without the need of post machining operations, (ii) its flexibility allows rapid prototyping and facilitates customizing components such as molds and tooling, and (iii) it reduces material wastage and is relatively inexpensive[1–3].

As a difference from traditionally manufactured FRP, thermoplastic matrices are commonly used in AM composites. This is mainly due to the thermal (low glass transition) and rheological (low viscosity) properties required for the preparation of the composite and the later additive deposition[4]. For approximately the past decade, short Fiber-Reinforced Thermoplastic (sFRT) composites, produced through additive manufacturing, have been extensively investigated[5–8]. Mainly, short fibers were added to reinforce pure raw polymeric materials such as Acrylonitrile Butadiene Styrene (ABS), Polylactide (PLA) and Nylon. However, the mechanical performance of these composites is in general limited, presenting a slightly higher strength and stiffness than the raw polymeric material. Hence, recent research trends are focusing on manufacturing new AM continuous Fiber-Reinforced Thermoplastic (cFRT) composites with carbon, glass, Kevlar and natural jute fibers. In contrast to sFRT, cFRT composites have the potential to substantially enhance the mechanical properties of printed components. For example, the tensile properties can be up to five times higher than that

of the unreinforced material[1,5,9]. There are several publications on the experimental analysis of cFRT under in-plane tension[10–15] and bending[11,16–19], but a lesser number of studies in the field of impact[20], fatigue and creep properties[21,22]. Currently, there is a lack of knowledge concerning the mechanical properties of cFRT under degrading environments, out-of-plane shear loading and, especially, about fracture toughness[23,24]. The latter is a relevant aspect for the mechanical performance of AM cFRT parts. In most of the manufacturing processes for AM composites, side-by-side filaments and layer-by-layer plies are deposited by a robotic system. Poor bonding between filaments of layers results in low interlaminar fracture toughness and low material performance.

Iragi et al.[25] carried out one of the first studies characterizing the interlaminar fracture toughness in mode I and mode II with 3D printed cFRT composites. The authors used the continuous Carbon Fiber (CF) reinforced PolyAmide 6 (PA) of the Markforged MarkTwo® system with Dyneema® doublers bonded to the bending arms of the specimen to prevent flexural failure during the tests. They found that the initiation value for the mode II fracture toughness (G_{IIc} = 1.59 kJ/m^2) was lower than that for mode I (G_{Ic} = 2 kJ/m^2). The authors justified this unusual material behavior by the large number of fiber bridges during mode I tests and the lack of matrix shearing in mode II tests. On the other hand, Santos et al.[26] characterized the interlaminar fracture toughness in mode I and mode II for the same CF/PA material, but without reinforcing the specimens with another composite or doubler. The authors concluded that the use of thicker specimens is not appropriate for this material type. They also found that the initiation value of the interlaminar fracture toughness in mode I (G_{Ic} = 1.5 kJ/m^2) was lower than the mode II fracture toughness (G_{IIc} = 1.95 kJ/m^2), which is the usual tendency for traditional laminated composite materials. In another study, Polyzos et al.[27] used PA doublers in specimens of the same material and obtained fracture toughness values in mode I and mode II similar to those of Santos et al.[26], 1.4 and 2 kJ/m^2, respectively. Moreover, Polyzos et al. used several analytical methods from the standards and 2D numerical models to predict the delamination process. They reported good agreement with the experimental results in mode II, while a significant error was found in mode I. This discrepancy was attributed to excessive fiber bridging, which is omitted in the analytical models.

One well-known limitation of the Markforged MarkTwo® system is the inability to control the printing parameters. To address this challenge, Goh et al.[28] employed an open-source 3D printer, the Hello BeePrusa, in conjunction with Markforged® cFRT material to investigate how printing parameters affect the mode I interlaminar fracture toughness of cFRT composites. Double Cantilever Beam (DCB) specimens were manufactured, and it was found that the highest fracture toughness (G_{Ic} = 943 J/m^2) was obtained under high nozzle and bed temperatures with low printing speed, 265 °C, 70 °C and 7 mm/s, respectively. The reported toughness was still lower than the published values using commercial 3D Markforged MarkTwo® printer[25–27,29]. Touchard et al.[29] analyzed the fracture toughness of both unidirectional (UD) and multidirectional (MD) 45/-45 CF/PA specimens under mode I loading using symmetric DCB specimens. Each laminate consisted of 20 PA plies and 2 CF/PA layers in each bending arm. To determine the interlaminar fracture toughness, the authors followed the experimental procedure proposed by Ozdil and Carlsson[30], according to which, the specimen is initially loaded until the interlaminar crack propagates approximately 5 mm. Subsequently, the specimen undergoes a series of unloading and reloading cycles. The interlaminar fracture toughness was 1.3 kJ/m^2, for the UD interface and 2.2 kJ/m^2 for the MD interface. According to Touchard and colleagues, the higher value of the interlaminar fracture toughness for the MD case aligns with the results found for carbon/epoxy laminates made from prepregs. However, delamination migration occurred after a few loading-unloading cycles for the MD specimens and only the initial points of the corresponding R-curves could be considered.

Kong et al.[31] analyzed experimentally the interlaminar fracture toughness under mixed-mode loading for cFRT CF/PA composites using the Single-Lap Shear (SLS) test. Pure mode I and mode II tests were also carried out. The stacking sequence for the pure mode loading specimens alternated between one Onyx® (short carbon fiber-reinforced PA) ply and one continuous CF ply along the arm thickness, whereas the SLS specimen (mixed-mode) changed the stacking sequence from one to two Onyx® layers. The fracture toughness was 1.1 and 0.49 kJ/m^2 for mode I and II, respectively. The latter was lower than the reported by Iragi et al.[25] using the same test, probably due to the different doublers and stacking sequence. For the SLS tests, the authors explored several material and interface angle combinations: CF/CF with 0/0, 90/90 and 0/90, CF/Onyx with 0/45, and Onyx/Onyx 45/-45. Macroscale fractography revealed a large area of intra-layer

separation for MD interfacing layers. Fiber fracture occurred at the end of the interface area for UD interface due to a better matrix impregnation during printing. The best balance between strength and flexibility was obtained for CF/CF cross-ply.

Katalagarianakis et al.[32] studied, for the first time, the interlaminar fracture toughness of cFRT CF/PA AM composites under a 50% mixed-mode $G_{II}/(G_I+G_{II})$ ratio, by performing Mixed-Mode Bending (MMB) tests. Pure mode I and mode II tests were also carried out. The authors determined the initiation values of the fracture toughness for mode I, 1.4 kJ/m^2, and mode II, 2.1 and 1.8 kJ/m^2, using the End-Loaded Split (ELS) and the End-Notched Flexure (ENF) tests, respectively. However, the initiation (1 kJ/m^2) and propagation (1.3 kJ/m^2) values for the mixed-mode toughness, were not in-between the pure mode I and II magnitudes, as it would have been expected. The authors were unable to explain this peculiar behavior and concluded that more research in this field is highly needed.

To date, the studies of Kong et al.[31] and Katalagarianakis et al.[32] are the only ones that have analyzed the fracture toughness of AM cFRT CF/PA material under mixed-mode loading. However, Kong et al. used the SLS test under which is not possible to clearly determine or control the degree of mixed-mode $G_{II}/(G_I+G_{II})$ involved. On the other hand, the initiation and propagation values reported by Katalagarianakis et al.[32] for the mixed-mode fracture toughness did not properly fall between the pure mode I and mode II loading, even using the well-established MMB test. As a result, additional research in this area is required, including the exploration of various mixed-mode ratios. To this end, in this work, we characterized experimentally the interlaminar fracture toughness of cFRT CF/PA AM composites using the MMB test, for three different mixed-mode $G_{II}/(G_I+G_{II})$ ratios: 25, 50 and 75%. The fracture toughness for the 50% mixed-mode ratio was found to be in-between the pure mode I and mode II values, as it is generally seen in traditional composite materials. Oppositely, the fracture toughness values for the MMB 25 and 75% tests were lower than that of mode I, which is not the expected tendency. A fracture surface exploration, using a scanning electron microscope, suggested that the values of fracture toughness obtained are unrelated to manufacturing defects or issues during testing.

The remainder of this paper is organized as follows. Firstly, we present the materials and the manufacturing process and preparation of the specimens, as well as the testing procedure. Secondly, results and discussion are presented. Finally, some conclusions are drawn.

2. Materials and methods

2.1. Specimens material and manufacturing

In this study, we utilized an AM unidirectional (UD) thermoplastic composite material obtained with Markforged MarkTwo® filament, combining continuous carbon fiber with PolyAmide 6, and referred to as CF/PA. The CF/PA material has a nominal ply thickness of 0.125 mm when using a solid infill pattern. Adjacent extruded rasters partially overlap by 250 μm, resulting in a width of 1.8 mm for two adjacent rasters[19]. The fiber volume fraction has a variability range between 27 and 41% with matrix and fiber dominated areas, random flaws and dry spot areas[14,18,25,33–37]. The in-plane elastic properties used to define testing parameters are as follows: longitudinal elastic modulus, E_{11} = 66.5 GPa, transverse elastic modulus, E_{22} = 6.1 GPa, and in-plane shear modulus G_{12} = 2.1 GPa. These properties were obtained in the AMADE laboratory following the corresponding ASTM standards[26].

The CF/PA specimens for the MMB tests with 25, 50 and 75% mixed-mode $G_{II}/(G_I+G_{II})$ ratios were designed and printed according to the ASTM-D6671[38] standard. Based on a previous experimental campaign performed by Santos et al.[26], the specimens for mode I and mode II loadings should have an arm thickness equal to 1.5 mm (3 mm in total) for the same material. This corresponds to a total of 24 plies (excluding the 4 top and bottom PA layers), with the fiber oriented in the longitudinal direction. Stable crack propagation was achieved during the entire test campaign using these DCB specimen dimensions and no stick-slip effect was observed[26]. Consequently, the same specimen thickness was used in this work.

Given the substantial amount of CF/PA composite material needed for this study, all specimens were individually manufactured with rounded corners to minimize residual thermal stresses and prevent warping effects. A larger PA brim than the default one in Eiger™ (slicer software from Markfoged®) was also defined to avoid debonding between the part and the printer bed. The number of the outer PA walls was set equal to

one, while the number of the floor layers was defined as four, which is the minimum imposed in Eiger™ under solid infill configuration. To generate the pre-crack at the midplane of the specimen, a Kapton® tape with a thickness of 50 μm was placed at the midplane after pausing the impression, following the procedure described by Santos et al.[26] (Figure 1). Following manufacturing, the printed specimens were stored in a dry box with desiccant bags at room temperature until they were instrumented and tested. This was done to prevent the moisture absorption by the Nylon and avoid any possible influence that it could have on the experimental results, such as a reduction in strength and stiffness, or an increase in ductility and impact resistance[39–41].

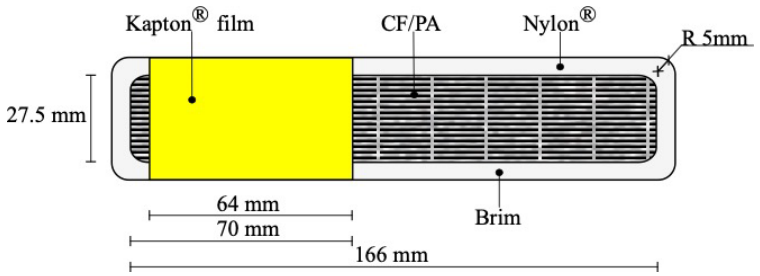

Figure 1. Schematic top view of the MMB specimen for fracture toughness exploration with the corresponding printed part dimensions.

Before testing, the specimens were post-processed by removing all PA walls and PA floor layers with a diamond saw. The MMB specimens had final dimensions of 160 mm × 25 mm × 3 mm (length × width × thickness), with a pre-crack length of 50 mm. In total, six MMB specimens were manufactured and tested for each of the considered loading ratios (25, 50 and 75%).

2.2. Testing

Figure 2 shows the testing equipment and tooling used to perform the MMB tests. The instrumented specimen was securely fastened to the base support and the load was applied vertically onto the upper lever. The mixed-mode ratio of the test was adjusted by altering the saddle position of the MMB fixture. The edges of the specimens were coated with white paint and 1 mm-spaced marks were drawn for monitoring the crack propagation. Two loading blocks, one at the top and one at the bottom, were attached to the cracked end of the specimen, following standard procedure (see Figure 2). In characterizing the 50% mixed-mode ratio, these

loading blocks were securely bonded by applying Henkel-Ibérica Loctite 401® on the surfaces, and no adhesion issues were encountered. However, during the 25 and 75% tests, the loading blocks at the cracked end experienced debonding under high loads. As a solution, the Henkel Loctite® EA 9466™ epoxy adhesive was used to bond the loading blocks for the remaining duration of the experimental campaign, resulting in successful outcomes.

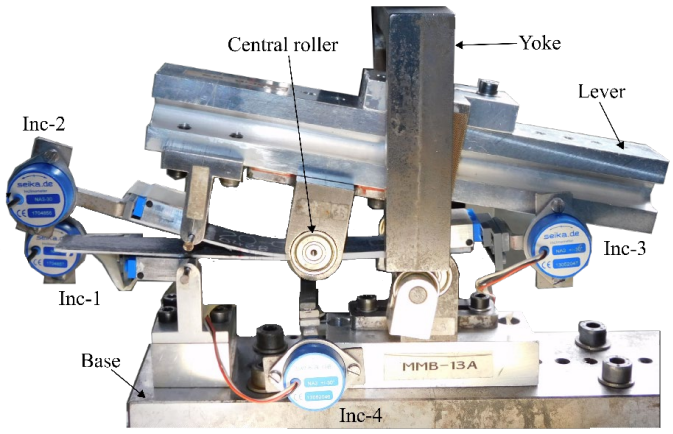

Figure 2. MMB specimen during testing instrumented with inclinometers (Inc-#).

As shown in Figure 2, four NA3-30 inclinometers, referred to as 'Inc-#', were used to facilitate the measurement of interlaminar fracture toughness using the J-integral method following the procedures outlined by Paris and Paris[42] and Sarrado et al.[43]. Nevertheless, during preliminary tests with 25 and 75% loading, it was observed that the Inc-4 inclinometer, attached to the underside of the specimen, experienced physical interference with the base fixture. This issue was especially pronounced for long crack lengths. Thus, this inclinometer had to be removed, and the J-integral method could not be used to determine the energy release rate. Instead, the modified beam theory method indicated in the standard[38] (based on Hashemi et al.[44] and Kinloch et al.[45]) was followed measuring the crack length during the tests. Thus, both initiation ($G_{II}/G_{c,ini}$) and propagation ($G_{II}/G_{c,prop}$) values were calculated.

All fracture tests were carried out using an MTS Insight testing machine equipped with a 5 kN load cell (calibrated for the full load range) at 23 ± 2 °C and 50 ± 5 HR. The cross-head speed of the system was set to 0.5 mm/min for loading and 2.5 mm/min for unloading. Since the thickness of the Kapton® insert exceeded

194 the thickness indicated in the standard[38] (13 µm), the initial pre-crack was extended for all the specimens
195 between 3 and 5 mm from the insert under mode I loading before the mixed-mode tests. This previous test
196 was carried out to avoid any possible effect of the tape and ensure the initiation from a sharp crack tip. During
197 all tests, force and displacement data were recorded. Crack propagation was monitored and recorded using a
198 high-resolution Canon® 5D reflex video camera.

199 ## 3. Results

200 The load-displacement curves for all MMB specimens tested at mixed-mode ratios of 25, 50 and 75% can be
201 seen in Figure 3 (25%), Figure 4 (50%) and Figure 5 (75%). Markers on the curves indicate the crack
202 propagation points as specified in the standard. All specimens exhibit a linear elastic response until the onset
203 of crack propagation, after which they display either a plateau or a softening behavior. The behavior of all of
204 them is analyzed and identified next.

205 ### 3.1. 25% mixed-mode ratio

206 As can be observed from the load-displacement curves in Figure 3, the entire batch of six MMB 25%
207 specimens was tested without any issues. All specimens exhibited smooth and stable crack growth throughout
208 the tests. However, the curves show different crack onset points and distinct behaviors during crack
209 propagation, with no clear trend emerging.

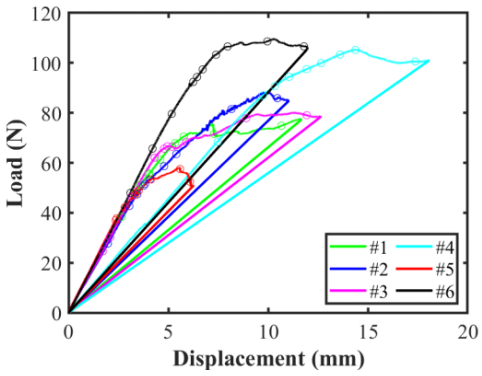

210

211 **Figure 3.** Load-displacement curves for the MMB 25% test.

It is noteworthy that the stiffness of specimen 25-4 was approximately 45% lower, and its maximum displacement was about 50% higher compared to the other specimens in the batch. All other specimens exhibited similar stiffness within the linear elastic region, although specimen 25-2 showed a secondary slope from a displacement of approximately 4 mm, once the delamination had started to propagate. Despite the differences among all the load-displacement curves, specimens 25-1, 25-2, and 25-3 exhibited more consistent results, showing similar stiffness prior and after crack propagation, as well as similar maximum force (between 81 and 92 N) and maximum displacement (between 11 and 13 mm).

On the other hand, specimen 25-5 exhibited the lowest load (62 N) and a maximum displacement of only 6 mm. Moreover, specimen 25-6 achieved the highest maximum load of 113 N and exhibited a maximum displacement comparable to that of specimens 25-1 to 25-3.

3.2. 50% mixed-mode ratio

Figure 4 presents the load-displacement curves for the 50% mixed-mode ratio batch. Monitoring of the crack propagation for the MMB 50% test was visually feasible up to a crack extension of approximately 35 mm. After that, the saddle had moved downward too much, covering the crack propagation at the edge of the specimen. Consequently, the specimens were unloaded once the crack reached this position. For this batch, all specimens exhibited a common trend, although specimens 50-2 and 50-6 demonstrated slightly lower stiffness.

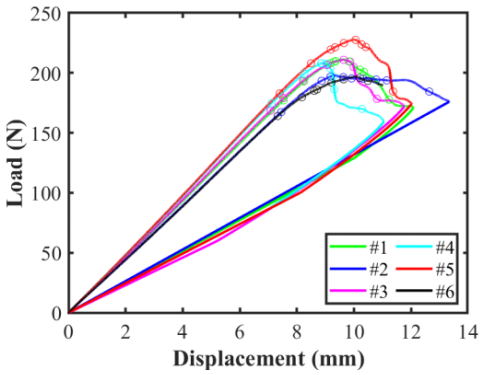

Figure 4. Load-displacement curves for the MMB 50% test.

It was possible to obtain a smooth and stable crack propagation for all the specimens up to a crack extension of 10 mm, except for specimen 50-6. In this case, the top loading block debonded from the specimen once the crack length had grown to about 5 mm after the peak load, and it was not possible to conclude the test. Nonetheless, this specimen is included for determining the fracture toughness since its mechanical response before this failure is in line with all the others. The MMB 50% batch showed an average maximum load and average maximum displacement of 217 N and 11.9 mm, respectively.

3.3. 75% mixed-mode ratio

The load-displacement curves for the 75% mixed-mode tests are shown in Figure 5. In general, this batch exhibited lower repeatability compared to the MMB 50% tests, but higher than the 25% ones. All specimens presented a similar curve, both during the linear elastic regime and during the crack propagation, except for specimens 75-4 and 75-6, which exhibited lower stiffness. As shown in the figure, the load-displacement curve of specimen 75-4 exhibited slightly lower stiffness and smaller stiffness difference between the loading and unloading phases compared to most of the specimens in the batch. Nevertheless, the peak load (289 N) and maximum displacement (6.3 mm) are in line with the average values of all other specimens, which were 270 N and 6.8 mm, respectively. However, similar to the situation found for the 25% mixed-mode tests, the stiffness of the load-displacement curve of specimen 75-6 was about 30% lower, while the peak load and maximum displacement were approximately 21% and 49% higher compared to the rest of the specimens in the batch.

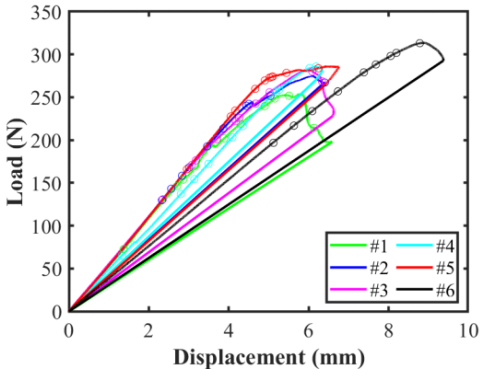

Figure 5. Load-displacement curves for the MMB 75% test.

The interlaminar fracture toughness results for mixed-mode loading ratios of 25, 50 and 75% in the CF/PA 3D printed composite are summarized in Table 1. As previously mentioned, specimens 25-4 and 75-6 exhibited stiffnesses in the linear part of their load-displacement curves that were 45% and 30% lower, respectively, than the rest of the specimens in their batches. Consequently, these specimens were excluded from the interlaminar fracture toughness analysis. Nevertheless, the individual calculation of the initiation and propagation values of the interlaminar fracture toughness for these two specimens yielded $G_{25\text{-}4,ini}$ = 1140 J/m^2 and $G_{25\text{-}4,prop}$ = 1800 J/m^2, and $G_{75\text{-}6,ini}$ = 1649 J/m^2 and $G_{75\text{-}6,prop}$ = 1893 J/m^2.

Table 1. Experimental values for the initiation and propagation interlaminar fracture toughness of the 3D printed CF/PA composite with mixed-mode ratios of 25, 50 and 75%.

$G_{II}/(G_I+G_{II})$ (%)	Fracture toughness (J/m^2)	
	Initiation	**Propagation**
25	318 ± 176	620 ± 283
50	1673 ± 133	2041 ± 153
75	323 ± 92	1143 ± 210

Despite undergoing identical manufacturing, preparation, conditioning, and testing procedures, specimens 25-4, 25-6 and 75-6 exhibited higher strength compared to the rest of the specimens in their batches. In contrast, specimen 25-5 showed lower strength. Furthermore, as previously mentioned, the stiffnesses observed for specimens 25-4 and 75-6 are lower than those of the other specimens in their respective batches. These variations imply that differing amounts of flaws originated during the manufacturing process, which may result in distinct mechanical behaviors. This inherent variability in material properties can be attributed to the pre-impregnated CF spool and the AM technology[26,46–48]. Indeed, previous studies have reported different values for in-plane elastic properties and interlaminar fracture toughness for the same CF/PA composite[25–28,49]. For instance, a higher void content could lead to a decrease in stiffness while simultaneously altering the interlaminar fracture toughness of the material. This hypothesis has been investigated in the following section through various microstructure analyses of the specimens.

4. Discussion

4.1. Fracture toughness variation and R-curves

Figure 6 summarizes the variation of the initiation and propagation fracture toughness versus the mixed-mode ratio. The figure includes the mode I and mode II interlaminar fracture toughness (G_{Ic} and G_{IIc}) obtained by Santos et al.[26] in a previous study for the same CF/PA composite material used in this work: $G_{Ic,ini}$ = 1497 J/m^2 and $G_{IIc,ini}$ = 1950 J/m^2 for initiation and $G_{Ic,prop}$ = 1720 J/m^2 and $G_{IIc,prop}$ = 2307 J/m^2 for propagation. As can be seen in the figure, only the fracture toughness values in the 50% mixed-mode MMB test fall within the range defined by the mode I and mode II. In contrast, the initiation and propagation fracture toughness values for the 25 and 75% mixed-mode ratios are notably lower than those of mode I, as clearly shown in Figure 6. The initiation values of the fracture toughness for both 25 and 75% mixed-mode ratios are approximately 21% of the mode I value. Moreover, the propagation fracture toughness of the 25 and 75% mixed-mode ratio are approximately 36% and 66%, respectively, of the mode I value.

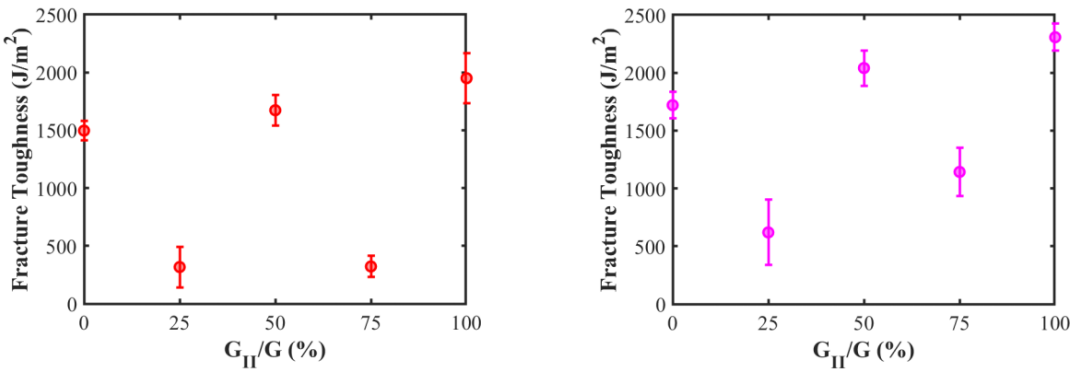

Figure 6. Variation of the initiation (left) and propagation (right) interlaminar fracture toughness of the AM CF/PA composite vs. the mixed-mode ratio. The fracture toughness values for mode I (0%) and mode II (100%) were reported by Santos et al.[26].

Generally, it is assumed that mode I fracture toughness is the most critical one and a conservative value for design purposes[50], especially for traditional composite materials, and that the fracture toughness value increases monotonically from mode I to mode II. However, Dillard et al.[51] summarized several cases where different authors reported mixed-mode fracture toughness values that were lower than those of mode I, with non-monotonic variations in fracture toughness between mode I and mode II. This is also the situation

reported by Katalagarianakis et al.[32] for the same material, manufacturing process and test method considered in the current study. In their work, Katalagarianakis et al. reported an initiation value of the critical energy release rate at a 50% mixed-mode ratio $G_{50c,ini}$ = 966 J/m^2, which was lower than the pure mode I, $G_{Ic,ini}$ = 1442 J/m^2, and pure mode II, $G_{IIc,ini}$ = 2130 J/m^2, values. A similar trend was reported for the propagation toughness values: $G_{Ic,prop}$ = 1853 J/m^2, $G_{50c,prop}$ = 1337 J/m^2 and $G_{IIc,prop}$ = 2275 J/m^2. Thus, although the variations of fracture toughness with the mixed-mode ratio shown in Figure 6 do not correspond to the usual situation, other studies have also observed non-monotonic trends.

Analyzing the different results, it can be observed that the behavior of the 50% mixed-mode ratio demonstrates good repeatability between tests, with a Coefficient of Variation (CV) of around 8% for both initiation and propagation (see Table 1). The 75% mixed-mode ratio results exhibit the second-best repeatability in terms of the load-displacement curves (see Figure 5). Consistent with this, this mixed-mode ratio also showed the second-lowest CV for initiation (28.5%) and propagation (18%). On the other hand, the MMB 25% batch exhibits the lowest repeatability in terms of load-displacement behavior. Consequently, it shows the highest CV for initiation and propagation fracture toughness values, 55% and 46%, respectively.

The crack propagation resistance curves (R-curve) for the MMB tests at 25, 50 and 75% are illustrated in Figure 7. The analysis of the R-curves reveals varying trends for different mixed-mode ratios. The 25% R-curve exhibits a clear linear trend, where increasing crack length corresponds to higher fracture toughness, without reaching a plateau. Consistent with the load-displacement curves shown in Figure 3, specimens 25-1 to 25-3 present similar behavior along the entire crack propagation length in the R-curve (Figure 7). Within this subgroup, the highest level of scatter is observed at the beginning of the curve, until a crack length of 55 mm. Beyond this point, the two longest crack lengths exhibit lower relative scatter. On the other hand, as shown in Figure 7, the lowest fracture toughness values across the crack propagation length for the MMB 25% batch correspond to specimen 25-5. This is consistent with the lowest peak load, maximum displacement and area under the load-displacement curve exhibited by this specimen, as seen in Figure 3. Conversely, specimen 25-6 presented the highest fracture toughness values across the crack propagation length for the

MMB 25% batch, which aligns with the highest peak load and area under the load-displacement curve of this specimen (Figure 3).

The initiation fracture toughness, measured at 318 J/m^2, correlates with the beginning of the curve. However, the propagation fracture toughness cannot be precisely identified due to the absence of the typical plateau observed in composite R-curves. Therefore, the mean fracture toughness value across all crack lengths, determined to be 620 J/m^2, can be considered a conservative estimate for design purposes.

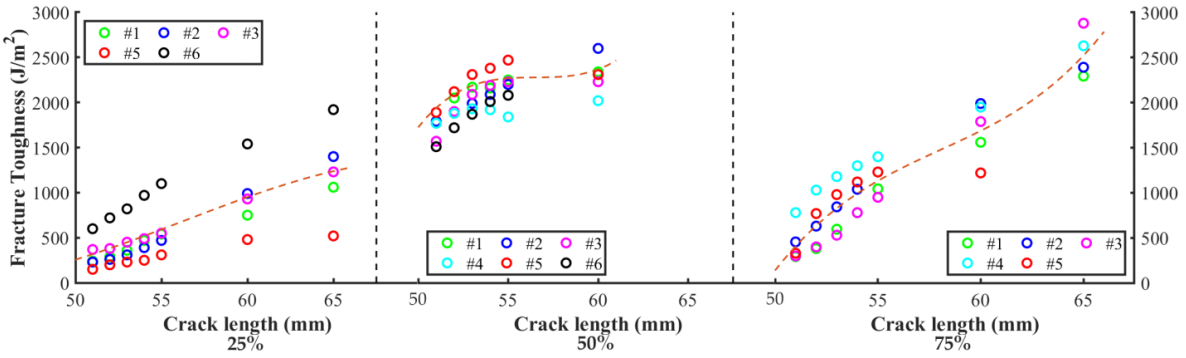

Figure 7. R-curves of the representative MMB specimens, separating each loading ratio through a vertical dashed black line. Red dashed curves correspond to trendlines obtained through a polynomial fit for each group.

In the case of the R-curve for the 50% mixed-mode ratio, an initial increasing trend is observed, with a plateau zone emerging after a crack length of 55 mm. Notably, specimen 50-4 exhibits a temporary decreasing trend at 54 and 55 mm crack lengths, but subsequently returns to an increasing trend. The initiation fracture toughness (1673 J/m^2) aligns with the onset of crack propagation at the beginning of the curve. In contrast, the propagation fracture toughness (2280 J/m^2) is located in the plateau zone, consistent with traditional laminated composite materials.

For the 75% mixed-mode ratio, the R-curve displays a doubly curved increasing trend, with higher fracture toughness values associated with longer crack lengths. This increasing tendency is particularly pronounced, with the initiation toughness (323 J/m^2) being nearly four times smaller than the propagation toughness (1143 J/m^2). However, significant scatter is observed along the entire test, especially at a crack length of 60 mm.

4.2. Fractographic analysis

To investigate whether the unexpectedly low fracture toughness values for the 25 and 75% mixed-mode ratios were due to manufacturing defects or material variability, a fractography analysis was conducted on representative post-mortem MMB specimens included in the interlaminar fracture toughness analysis. Each specimen was manually split open, and the first 20 mm of crack propagation length was carefully cut to preserve the original failure morphology. A scanning electron microscope (SEM) was employed for microscopic failure analysis, using an accelerating voltage of 7 kV. To enhance scanning quality, the bottom surface of each specimen was adhered with conductive tape and rendered conductive through carbon evaporation using an Emitech K950® system.

As can be seen in Figure 8, at lower magnification, all fracture surfaces exhibit irregularities, indicating that the fiber filament rasters deposited during manufacturing are not perfectly straight. Instead, they exhibit a waviness along the continuous fiber direction, denoted by the dashed blue lines along the longitudinal crack propagation in Figure 8a, Figure 8c and Figure 8e. These rasters create longitudinal furrows in all specimens, resulting in darker areas alongside lighter ones in the MMB 25 and 75% specimens. Some loose, long fibers are also visible in all micrographs, particularly in the MMB 75% specimen. Additionally, white PA particles surrounded by small dark areas are randomly deposited on the surfaces, with the 50% test displaying the highest irregular surface and, consequently, the highest number of air bubbles or voids between adjacent longitudinally deposited fiber filaments. The MMB 25% specimen exhibits the smoothest surface, with distinct matrix-dominated areas (darker longitudinal regions) situated between the fiber-dominated ones (lighter areas). It is noteworthy that the MMB 25 and 75% specimens share relatively similar fracture morphology.

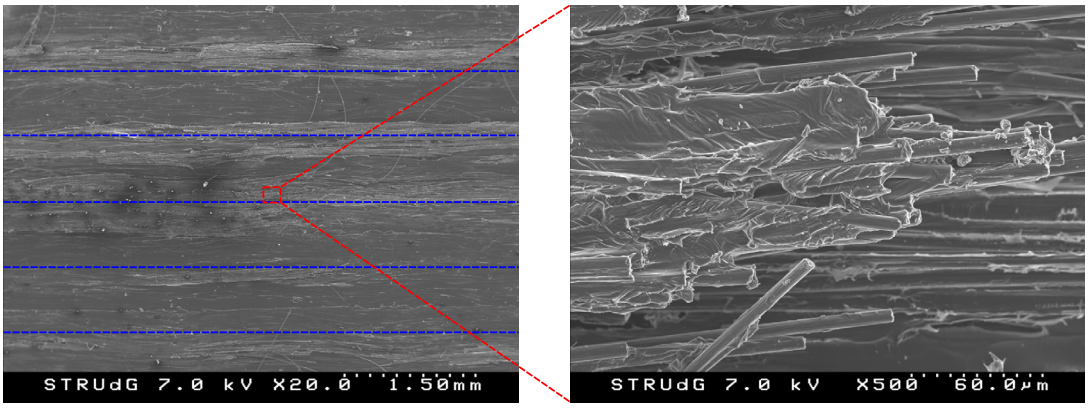

a) 25% test with the smoothest surface **b)** Close-up of a MMB 25% test

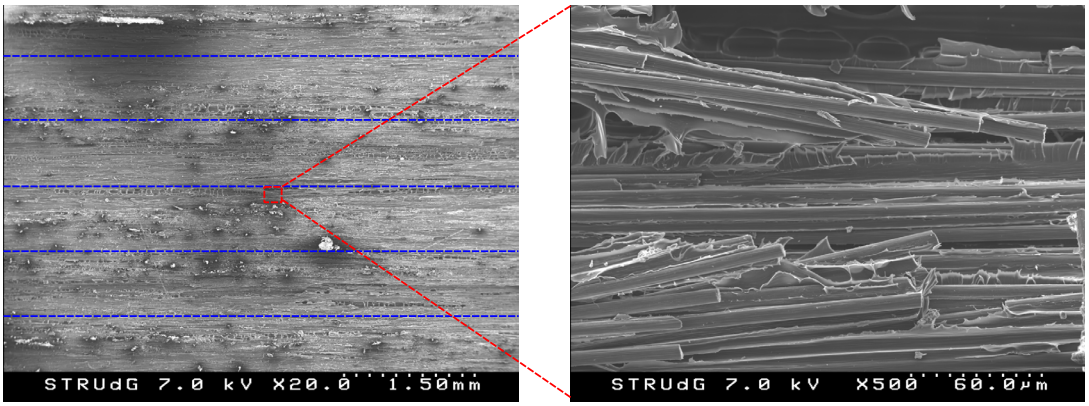

c) 50% test showed the highest irregularity **d)** Close-up of a MMB 50% test

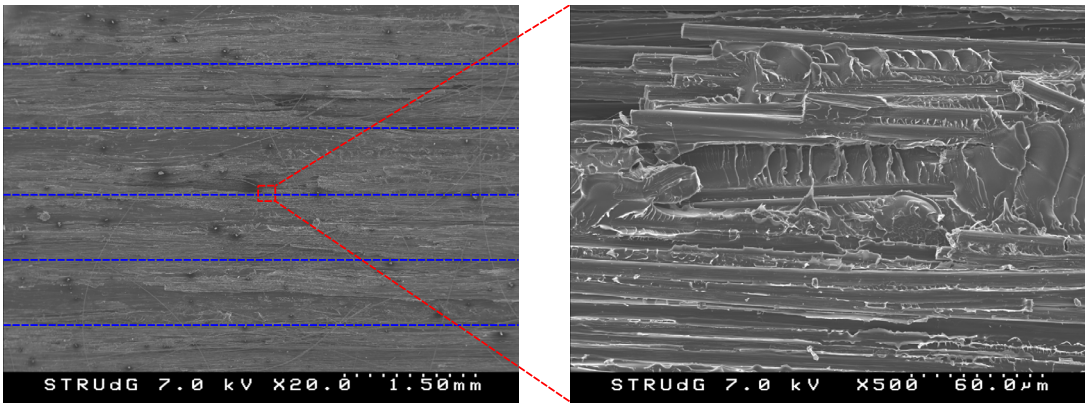

e) 75% test with longest loose broken fibers **f)** Close-up of a MMB 75% test

Figure 8. SEM images of the fracture surfaces of the representative MMB 25, 50 and 75% specimens analyzed at two different levels of magnification.

A higher magnification analysis was conducted on the fracture surfaces of specimens subjected to MMB 25, 50 and 75% tests, as illustrated in Figure 8b, Figure 8d and Figure 8f, respectively. In all micrographs, inadequate impregnation of the fiber with PA is evident, with the lowest impregnation observed in the case of the MMB 50% test (Figure 8d) consistent with the presence of voids observed at lower magnification. Fiber misalignment is also noticeable in all specimens after testing.

In the case of the MMB 25% (Figure 8b), a tow of broken fibers partially covered with PA is observed, revealing matrix deformation in the form of ridges. This fracture morphology corresponds to a lower amount of mode II (i.e., lesser sliding) for this mixed-mode, with broken fibers dominating the image. The close-up of the MMB 50% test (Figure 8d) reveals both broken fibers and plastic deformation in the form of inclined ridges on the upper plane of the image. At a deeper plane, evidence of fiber-matrix debonding, plastic deformation, fiber breakage, and irregular spaces between fibers can be identified. The amplified image for the MMB 75% specimen (Figure 8f) shares similarities with that of the 25% specimen as highlighted previously at lower magnification. However, a larger area of shear plastic deformation is observed in the 75% specimen compared to the 25 and 50% ratios, indicating a higher proportion of mode II due to increased sliding between arms. Few traces of debonded fibers are observed within the PA matrix.

The fracture surfaces of specimens 25-4 and 75-6, which were excluded from the interlaminar fracture toughness analysis, were inspected using SEM, following the same procedure as for the other specimens. The fracture surfaces for these specimens are shown in Figure 9. At lower magnification, it can be observed that the level of air bubbles or voids between adjacent rasters is higher in both specimens compared to what is seen in Figure 8 for the MMB 25 and 75% specimens. Additionally, it can be observed that the fracture surface of the 25% specimen contains many long loose fibers, whereas fewer are seen for specimen 75-6. At higher magnification, both fracture surfaces reveal non-impregnated fibers, but this is more pronounced for specimen 25-4. On the other hand, the fracture surface presented in Figure 9b shows more matrix deformation in the form of ridges, which is typically associated to a higher contribution of mode I. In contrast, the fracture surface in Figure 9d displays more shear plastic matrix deformation, indicating a higher proportion of mode II. The distinctive features observed in the SEM images of the fracture surfaces of these two specimens,

compared to those of the other specimens tested under the same mixed-mode ratio, may explain their lower stiffness and higher fracture toughness. To further explore this hypothesis, a microstructure analysis has been conducted in the following section.

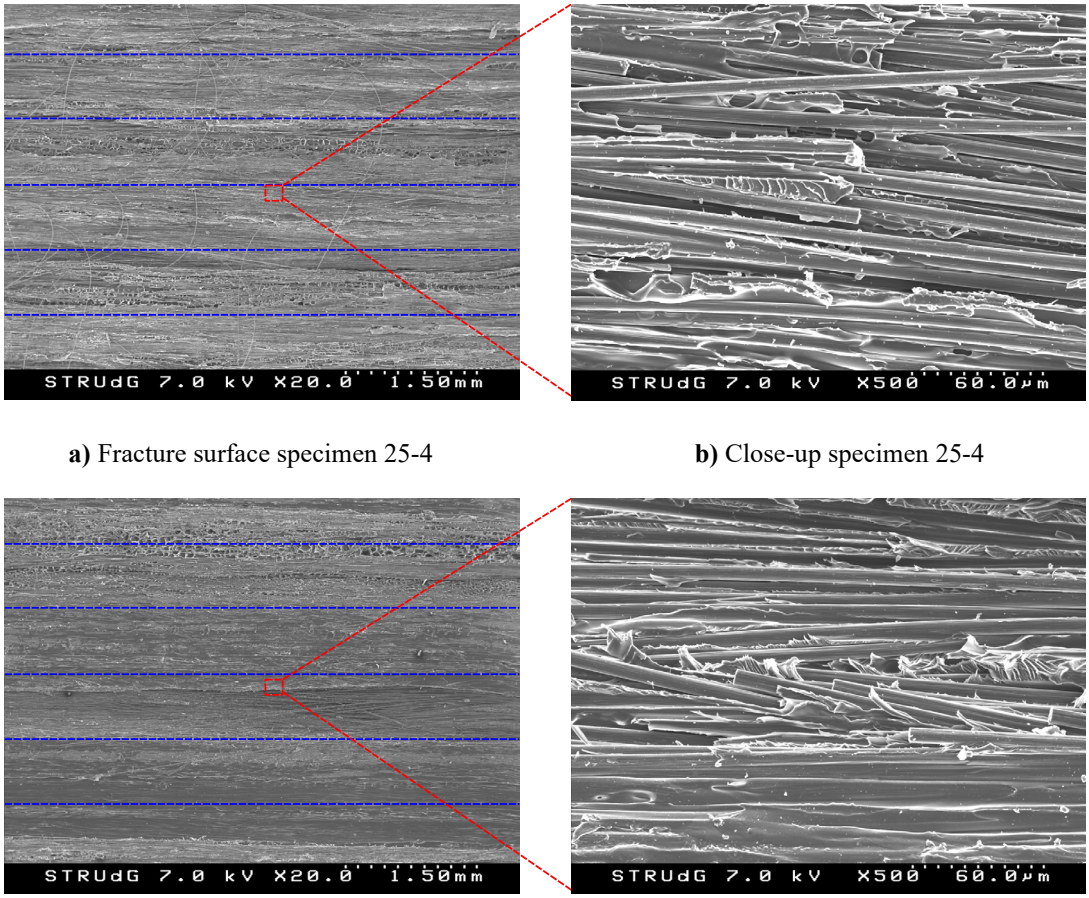

a) Fracture surface specimen 25-4 **b)** Close-up specimen 25-4

c) Fracture surface specimen 75-6 **d)** Close-up specimen 75-6

Figure 9. SEM images of the fracture surfaces of specimens 25-4 and 75-6 analyzed at two different levels of magnification.

4.3. Microstructure analysis

A microstructure analysis of representative post-mortem specimens under 25, 50 and 75% mixed-mode ratios was carried out using the EN 2564[52] standard for a better interpretation of the results. The mass and volume fractions of fiber and matrix, as well as the void content, for the three mixed-mode ratios are summarized in Table 2. It can be observed in this table that fiber and matrix mass fractions were virtually the same for the three mixed-mode ratios. There was more variation in fiber and matrix volume fractions between mixed-mode

ratios, but differences were less than 8 and 9%, respectively. However, the void content values varied considerably between mixed-mode ratios. Indeed, the lowest void content was found for the MMB 75% specimen, 8.3%, while, the highest void content, 16.1%, was found for the MMB 50% specimen, approximately 94% more. This is in line with the observations from the SEM analysis, where indications of higher presence of voids or air bubbles were already detected for the MMB 50% specimens. It is worth noting that this porosity level is within the range of values reported by other authors for the same material and 3D printer: Yavas et al.[53] 3.4%, Iragi et al.[25] 7.5%, He et al.[54] 12%, Chabaud et al.[34] 15% and Saaed et al.[55] 20%.

Table 2. Fiber, matrix and void content of the MMB 25, 50 and 75% specimens.

$G_{II}/(G_I+G_{II})$ (%)	Fiber fraction (%)		Matrix fraction (%)		Void fraction (%)
	Mass	Volume	Mass	Volume	Volume
25	44.4	28.6	55.6	58.7	12.7
50	44.8	27.8	55.2	56.1	16.2
75	44.6	30.2	55.4	61.5	8.3

The same microstructure analysis was performed on the two specimens excluded from the interlaminar fracture toughness analysis due to their low stiffness: specimen 25-4 and specimen 75-6. The results obtained for these two specimens are summarized in Table 3. It can be observed that in comparison to the values included in Table 2, the fiber mass fraction was higher, while the matrix one was lower. Furthermore, while the fiber volume fractions are comparable, there is a reduction in matrix volume fraction. This resulted in higher void contents. This agrees with the indications of air bubbles or voids in the fracture surfaces shown in Figure 9. These higher void fractions were likely responsible for the reduction in stiffness observed in these specimens. However, the reduction in stiffness was not directly proportional to the increase in void content. For instance, while the stiffness reduction for specimen 25-4 was of 45% with respect to the rest of specimens in the batch, its increase in void content was 29%. On the other hand, for specimen 75-6 the stiffness reduction was about 30% and the void content increase was 169%. In parallel, and as will be discussed later, the higher void content observed in these two specimens compared to the other specimens in their respective batches might be considered a possible cause for their higher interlaminar fracture toughness.

Table 3. Fiber, matrix and void content of specimens 25-4 and 75-6.

Specimen	Fiber fraction (%)		Matrix fraction (%)		Void fraction (%)
	Mass	Volume	Mass	Volume	Volume
25-4	46.4	28.9	53.6	54.7	16.4
75-6	45.8	26.5	54.2	51.2	22.3

The microstructure of representative specimens included in the fracture toughness analysis was also analyzed through SEM observations of the cross-sections of one beam of specimen per mixed-mode ratio (Figure 10). It can be clearly observed in the micrographs of the three cross-sections that there was an accumulation of voids where consecutive filament rasters overlap. In line with the measurement of the void contents previously commented, the density of voids was lower for the MMB 75% specimen, approximately 3.8% (Figure 10c and Figure 10f). However, for the specific cross-sections considered, and opposite to the determination of the voids content according to the EN 2564 standard, the area of voids observed for specimen 25% (Figure 10a and Figure 10d), 9.2%, was larger than the one corresponding to the MMB 50% specimen (Figure 10b and Figure 10e), 7.3%.

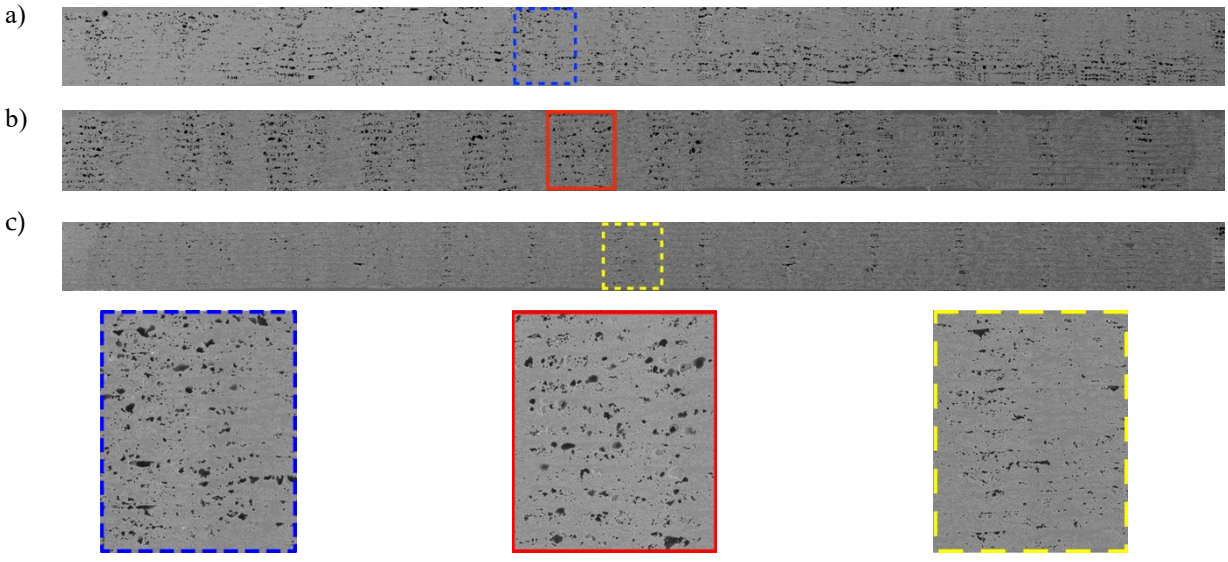

Figure 10. SEM micrographs of the cross-sections of representative MMB a) 25%, b) 50% and c) 75% specimens and the corresponding closeups.

435 The analysis of the fracture surface and the microstructure of the MMB specimens revealed differences in
436 porosity. Additionally, the two specimens excluded from the interlaminar fracture toughness analysis showed
437 variations in fiber and matrix volume fractions. Nevertheless, it is not totally clear to what extent the
438 differences in void content may have affected the interlaminar fracture toughness values obtained for each
439 mixed-mode ratio, as well as the stiffness response.

440 On the one hand, He et al.[54] compared the tensile response of 3D-printed prismatic specimens manufactured
441 with the same material with and without compression molding (CM) post-processing, applying a pressure of 5
442 MPa, for 10 minutes at 230 ºC. They observed that the porosity level was reduced from 11 to 3.4%, while the
443 tensile modulus increased from 61 to 83 MPa and the tensile strength increased from 767 to 940 MPa. Saeed
444 et al.[56] followed a similar procedure but kept the same pressure for 60 minutes at 130 ºC. In this case, the final
445 value of void content was 3.96%, while the final values of tensile modulus and strength, 768 MPa and 80
446 GPa, respectively, were 27% higher in comparison to the values achieved without post-processing.

447 In their work, He et al.[54] also reported differences in the measure of the mode I fracture toughness. They
448 found that the initiation value increased from 118.5 to 225 J/m^2, whereas the propagation one was reduced
449 from 1467 to 471 J/m^2. The analysis of the fracture surfaces revealed that the higher volume of voids in the
450 non-postprocessed specimens facilitated the debonding between matrix and fibers. Thus, a major proportion
451 of fiber bridging occurred and the fracture toughness during propagation increased. Similarly, Iragi[57] observed
452 a reduction in the mode I fracture toughness for the same material, from 1886 to 250 J/m^2, when it was
453 postprocessed at 210 ºC and 1 MPa for 15 minutes. Iragi also observed that the fracture surface of the non-
454 postprocessed specimens was more irregular and involved more fiber bridging that in the case of the
455 postprocessed ones. According to this, the interlaminar fracture toughness of the 25 and 50% specimens
456 should be higher than that of the 75% specimens, as the micrographs presented in Figure 8 show a more
457 irregular microstructure and more broken fibers (resulting from fiber bridging) for the former. However, the
458 fracture toughness found for the MMB 75% specimens in propagation was approximately twice that of the
459 25% ones.

460 On the other hand, Iragi[57] also reported an increase in the mode II fracture toughness, from 1590 to 1801 J/m^2,
461 when the material was postprocessed under the same conditions (210 ºC and 1 MPa for 15 minutes). In this
462 case, the fracture surface of the postprocessed specimens involved more shear failure cracks in the matrix.
463 Thus, in our case, the fracture toughness of the 75% mixed-mode ratio specimens should be higher than that
464 of the 50% ones: less void content and higher component of mode II. However, the value of the interlaminar
465 fracture toughness found for the MMB 50% specimens was 79% higher than that of the 75% ones.
466 Considering specimens 25-4 and 75-6, which were excluded from the fracture toughness analysis, the higher
467 void content compared to the other MMB 25 and 75% specimens, respectively, could be related to the
468 increase in fracture toughness. Specifically, an increase in porosity of 29% for specimen 25-4 resulted in a
469 258% increase in fracture toughness for initiation and a 190% increase for propagation. For specimen 75-6, an
470 increase in porosity of 169% led to a 411% increase in fracture toughness for initiation and a 66% increase for
471 propagation.

472 Consequently, it seems evident that the level of porosity in the specimens had an effect in the stiffness
473 response and interlaminar fracture toughness of the specimens. However, it has not been possible to establish
474 a clear and univocal association between void content and variation in stiffness and fracture toughness.

475 In the present study, all specimens were manufactured with the same 3D printer, using the same Markforged®
476 material and following the same manufacturing procedure. The only reasons for different void contents can be
477 the variations in the CF spools used to manufacture the specimens and the relatively low repetitiveness
478 associated to 3D printing processes resulting in a wide range of reported values for the same material
479 properties (as summarized by Santos et al.[26]). These two factors would also explain the difference in the value
480 of the 50% mixed-mode interlaminar fracture toughness measured in this work, 2041 J/m^2, and the one
481 reported by Katalagarianakis et al.[32], 1300 J/m^2, a reduction of 36%, while the values for pure mode I and
482 pure mode II were similar. In these two works, the void contents in the specimens were not reported and,
483 therefore, it is not possible to establish a clear relation between void content and interlaminar fracture
484 toughness. The same variability and low repetitiveness of the manufacturing process could explain the high

485 void contents observed in specimens 25-4 and 75-6 in parallel to a reduction in stiffness and an increase in
486 fracture toughness in comparison to the other specimens in their respective batches.

487 Overall, this study demonstrates the successful manufacturing and testing of additive manufacturing CF/PA
488 composite specimens for MMB 25, 50 and 75% mixed-mode tests, following traditional laminated composite
489 material guidelines. However, it is noteworthy that there was no clear trend in fracture toughness values as a
490 function of the mixed-mode ratio. While the fracture toughness for a 50% mixed-mode ratio fell between
491 mode I and mode II values, the 25 and 75% ratios exhibited toughness values lower than mode I. Although
492 this is not the usual behavior in the case of composite materials, different authors[32,51] have reported mixed-
493 mode fracture toughness values lower than that of mode I and non-monotonic variations of the fracture
494 toughness values with the mixed-mode ratio. Hence, several key points can be highlighted from this work:

495 - To the authors' best knowledge, this is one of the first works investigating the interlaminar fracture
496 toughness using the MMB test with additive manufacturing thermoplastic CF/PA composites and the first to
497 consider 25 and 75% mixed-mode ratios. Previously, Kong et al.[31] evaluated the fracture toughness under
498 mixed mode of CF/PA material, but the authors used a less common SLS specimen and focused on a single
499 mixed mode ratio.

500 - The present work revealed a peculiar behavior in the fracture toughness values, which contradicted the
501 typical trend observed in traditional composite materials. For a 50% mixed-mode ratio, the fracture toughness
502 fell between mode I and mode II, aligning with expectations. However, for the 25 and 75% ratios, the fracture
503 toughness was lower than in mode I.

504 - Katalagarianakis et al.[32] characterized the same CF/PA material using the MMB test under a 50% mixed
505 mode ratio, obtaining that the initiation and propagation fracture toughness values were lower than the pure
506 mode I ones. Hence, the findings of the present work contribute to further increase the knowledge of the
507 mechanical performance of this additive manufacturing composite material.

- SEM and microstructure analyses proved that the void content was higher for the MMB 50% specimens and lower for the 75% ones, with the 25% ones in between. Additionally, high void fractions were observed in the two specimens with reduced stiffness response and higher interlaminar fracture toughness.

- The findings of this work highlight a dependency of mixed-mode interlaminar fracture toughness values on the void content in the specimens. Nevertheless, it has not been possible to establish a clear and definite relation between the void content and the possible variation in the value of fracture toughness. More fracture toughness tests should be carried out in a future work including specimens in mode I, mode II and different mixed-mode ratios ensuring homogeneous and representative fractions of voids across all the batches of specimens.

- Considering that the amount of fiber bridging present in the specimens can be affected by interfacial bonding between fiber and matrix, it would be worth characterizing this property in a future work, e.g. using the push-in or push-out tests.

5. Conclusions

Mixed-Mode Bending (MMB) tests with mixed-mode ratios of 25, 50 and 75%, were carried out to determine the initiation and propagation interlaminar fracture toughness of an additive manufacturing cFRT CF/PA composite material. The following findings can be summarized.

The MMB 50% case showed the highest repeatability response of the entire investigation. Moreover, the fracture toughness for the 50% mixed-mode ratio fell between the values for pure mode I and mode II, $G_{50c,ini}$ = 1673 J/m^2 and $G_{50c,prop}$ = 2041 J/m^2, which would correspond to the typical monotonic variation of interlaminar fracture toughness. In contrast, the fracture toughness for the MMB 25 and 75% tests was lower than that of mode I. For all mixed-mode ratios, an increasing tendency was identified on the analysis of the R-curve. Nonetheless, while for the 50% mixed-mode ratio the R-curve showed a plateau region for longer crack lengths, this response has not been observed for the 25 and 75% tests. Consequently, the propagation fracture toughness for the MMB 75% ratio was nearly 4 times higher than the initiation value.

A microscopic fractography analysis revealed the MMB 50% surface was more irregular, damaged, and had a larger presence of voids than for the 25 and 75% specimens. Nonetheless, the 25 and 75% specimens also presented significant irregularities and voids. The 25% specimen showed the smoothest surface with the major PA dominant longitudinal raster areas. The 75% specimen had the highest quantity of long loose fibers after the test. Analyzing the images at a higher magnification, the dominant failure mechanism was properly observed for each loading ratio. More quantity of broken fibers, due to delamination, were observed for 25%, a proper balance between opening and shearing was seen in the 50% case, with broken fiber and permanent plastic deformation in shear, whereas the 75% showed dominated plastic shear deformation with few broken fibers. The microstructure analysis revealed a higher void content for the MMB 50% specimens, 16%, and a lower one for the 75% specimens, 8%, with most of the voids concentrated in the overlaps of the fiber filament rasters.

Two specimens, one tested at a 25% mixed-mode ratio and the other at 75%, exhibited significantly lower stiffness responses compared to the rest of the specimens in their batches, alongside increased fracture toughness values. The microstructure analysis of these specimens revealed higher void fractions compared to the rest of specimens in their batches, establishing a dependency between void content and propagation fracture toughness. This dependency confirms the influence of the low repetitiveness of the manufacturing process on void content and material properties. However, it has not been possible to establish a clear relationship between the variation in the measured interlaminar fracture toughness values and the porosity in the specimens. Thus, it would be worthwhile considering future work focusing on a comprehensive experimental characterization of the interlaminar fracture toughness, ensuring homogeneous and representative void contents across all the batches of specimens.

Finally, although it has not been possible to establish a clear correlation between the atypical non-monotonic variation of the interlaminar fracture toughness and the void content in the material, it should be considered that this can be a possible and intrinsic characteristic of the material and possible users should be aware of it.

Acknowledgments

This research was funded by the Spanish Ministry of Science, Innovation and versities (MCIU), the Spanish Research Agency (AEI) and the European Regional Development Fund (FEDER, UE) (grant no. RTI2018-094435-B-C32 and PID2022-140343NB-100). **José M. Guerrero** would also like to acknowledge the funding of the post-doc grant Margarita Salas with reference (grant no. REQ2021_A_15) financed by the Spanish 'Ministerio de Universidades' and the European Union - Next GenerationEU. **Jonnathan D. Santos** acknowledges the support from the research group ATEI at Universidad Politécnica Salesiana and technical support from the research group AMADE at Universitat de Girona.

References

1. Liu G, Xiong Y, Zhou L. Additive manufacturing of continuous fiber reinforced polymer composites: Design opportunities and novel applications. *Composites Communications*. 2021;27(July):100907. doi:10.1016/j.coco.2021.100907

2. Li J, Durandet Y, Huang X, Sun G, Ruan D. Additively manufactured fiber-reinforced composites: A review of mechanical behavior and opportunities. *J Mater Sci Technol*. 2022;119:219-244. doi:10.1016/j.jmst.2021.11.063

3. Brenken B, Barocio E, Favaloro A, Kunc V, Pipes RB. Fused filament fabrication of fiber-reinforced polymers: A review. *Addit Manuf*. 2018;21:1-16. doi:10.1016/j.addma.2018.01.002

4. Zhuo P, Li S, Ashcroft IA, Jones AI. Material extrusion additive manufacturing of continuous fibre reinforced polymer matrix composites: A review and outlook. *Compos B Eng*. 2021;224. doi:10.1016/j.compositesb.2021.109143

5. Goh GD, Yap YL, Agarwala S, Yeong WY. Recent Progress in Additive Manufacturing of Fiber Reinforced Polymer Composite. *Adv Mater Technol*. 2019;4(1). doi:10.1002/admt.201800271

6. Aliheidari N, Tripuraneni R, Ameli A, Nadimpalli S. Fracture resistance measurement of fused deposition modeling 3D printed polymers. *Polym Test*. 2017;60:94-101. doi:10.1016/j.polymertesting.2017.03.016

7. Young D, Wetmore N, Czabaj M. Interlayer fracture toughness of additively manufactured unreinforced and carbon-fiber-reinforced acrylonitrile butadiene styrene. *Addit Manuf*. 2018;22:883-890. doi:10.1016/j.addma.2018.02.010

8. Khudiakova A, Arbeiter F, Spoerk M, Wolfahrt M, Godec D, Pinter G. Inter-layer bonding characterisation between materials with different degrees of stiffness processed by fused filament fabrication. *Addit Manuf*. 2019;28:184-193. doi:10.1016/j.addma.2019.05.006

9. Blok LG, Longana ML, Yu H, Woods BKS. An investigation into 3D printing of fibre reinforced thermoplastic composites. *Addit Manuf*. 2018;22:176-186. doi:10.1016/j.addma.2018.04.039

10. Melenka GW, Cheung BKO, Schofield JS, Dawson MR, Carey JP. Evaluation and prediction of the tensile properties of continuous fiber-reinforced 3D printed structures. *Compos Struct*. 2016;153:866-875. doi:10.1016/j.compstruct.2016.07.018

11. Dickson AN, Barry JN, McDonnell KA, Dowling DP. Fabrication of continuous carbon, glass and Kevlar fibre reinforced polymer composites using additive manufacturing. *Addit Manuf*. 2017;16:146-152. doi:10.1016/j.addma.2017.06.004

12. Pyl L, Kalteremidou KA, Van Hemelrijck D. Exploration of specimen geometry and tab configuration for tensile testing exploiting the potential of 3D printing freeform shape continuous carbon fibre-reinforced nylon matrix composites. *Polym Test*. 2018;71(September):318-328. doi:10.1016/j.polymertesting.2018.09.022

13. Zappino E, Filippi M, Pagani A, Petiti M, Carrera E. Experimental and numerical analysis of 3D printed open-hole plates reinforced with carbon fibers. *Composites Part C: Open Access*. 2020;2. doi:10.1016/j.jcomc.2020.100007

14. Justo J, Távara L, García-Guzmán L, París F. Characterization of 3D printed long fibre reinforced composites. *Compos Struct*. 2018;185:537-548. doi:10.1016/j.compstruct.2017.11.052

15. Rimkus A, Farh MM, Gribniak V. Continuously Reinforced Polymeric Composite for Additive Manufacturing—Development and Efficiency Analysis. *Polymers (Basel)*. 2022;14(17). doi:10.3390/polym14173471

16. Dikshit V, Nagalingam AP, Goh GD, Agarwala S, Yeong WY, Wei J. Quasi-static indentation analysis on three-dimensional printed continuous-fiber sandwich composites. *Journal of Sandwich Structures and Materials*. 2021;23(2):385-404. doi:10.1177/1099636219836058

17. Araya-Calvo M, López-Gómez I, Chamberlain-Simon N, et al. Evaluation of compressive and flexural properties of continuous fiber fabrication additive manufacturing technology. *Addit Manuf*. 2018;22:157-164. doi:10.1016/j.addma.2018.05.007

18. Chacón JM, Caminero MA, Núñez PJ, García-Plaza E, García-Moreno I, Reverte JM. Additive manufacturing of continuous fibre reinforced thermoplastic composites using fused deposition modelling: Effect of process parameters on mechanical properties. *Compos Sci Technol*. 2019;181. doi:10.1016/j.compscitech.2019.107688

19. Goh GD, Dikshit V, Nagalingam AP, et al. Characterization of mechanical properties and fracture mode of additively manufactured carbon fiber and glass fiber reinforced thermoplastics. *Mater Des*. 2018;137:79-89. doi:10.1016/j.matdes.2017.10.021

20. Caminero MA, Chacón JM, García-Moreno I, Rodríguez GP. Impact damage resistance of 3D printed continuous fibre reinforced thermoplastic composites using fused deposition modelling. *Compos B Eng*. 2018;148(April):93-103. doi:10.1016/j.compositesb.2018.04.054

21. Mohammadizadeh M, Imeri A, Fidan I, Elkelany M. 3D printed fiber reinforced polymer composites - Structural analysis. *Compos B Eng*. 2019;175. doi:10.1016/j.compositesb.2019.107112

22. Brooks H, Tyas D, Molony S. Tensile and fatigue failure of 3D printed parts with continuous fibre reinforcement. *International Journal of Rapid Manufacturing*. 2017;6(2/3):97. doi:10.1504/ijrapidm.2017.082152

23. Díaz-Rodríguez JG, Pertúz-Comas AD, González-Estrada OA. Mechanical properties for long fibre reinforced fused deposition manufactured composites. *Compos B Eng*. 2021;211. doi:10.1016/j.compositesb.2021.108657

24. Khosravani MR, Berto F, Ayatollahi MR, Reinicke T. Fracture behavior of additively manufactured components: A review. *Theoretical and Applied Fracture Mechanics*. 2020;109. doi:10.1016/j.tafmec.2020.102763

25. Iragi M, Pascual-González C, Esnaola A, Lopes CS, Aretxabaleta L. Ply and interlaminar behaviours of 3D printed continuous carbon fibre-reinforced thermoplastic laminates; effects of processing conditions and microstructure. *Addit Manuf*. 2019;30. doi:10.1016/j.addma.2019.100884

26. Santos JD, Fernández A, Ripoll L, Blanco N. Experimental Characterization and Analysis of the In-Plane Elastic Properties and Interlaminar Fracture Toughness of a 3D-Printed Continuous Carbon Fiber-Reinforced Composite. *Polymers (Basel)*. 2022;14(3). doi:10.3390/polym14030506

27. Polyzos E, Katalagarianakis A, Van Hemelrijck D, Pyl L. Delamination analysis of 3D-printed nylon reinforced with continuous carbon fibers. *Addit Manuf*. 2021;46. doi:10.1016/j.addma.2021.102144

28. Goh GD, Dikshit V, An J, Yeong WY. Process-structure-property of additively manufactured continuous carbon fiber reinforced thermoplastic: an investigation of mode I interlaminar fracture toughness. *Mechanics of Advanced Materials and Structures*. 2020;29(10):1418-1430. doi:10.1080/15376494.2020.1821266

29. Touchard F, Chocinski-Arnault L, Fournier T, Magro C, Lafitte A, Caradec A. Interfacial adhesion quality in 3D printed continuous CF/PA6 composites at filament/matrix and interlaminar scales. *Compos B Eng*. 2021;218. doi:10.1016/j.compositesb.2021.108891

30. Ozdil F, Carlsson LA. Beam analysis of angle-ply laminate DCB specimens. *Compos Sci Technol*. 1999;(59):305-315. doi:10.1016/S0266-3538(98)00069-4

31. Kong X, Luo J, Luo Q, Li Q, Sun G. Experimental study on interface failure behavior of 3D printed continuous fiber reinforced composites. *Addit Manuf*. 2022;59. doi:10.1016/j.addma.2022.103077

32. Katalagarianakis A, Polyzos E, Van Hemelrijck D, Pyl L. Mode I, mode II and mixed mode I-II delamination of carbon fibre-reinforced polyamide composites 3D-printed by material extrusion. *Compos Part A Appl Sci Manuf*. 2023;173. doi:10.1016/j.compositesa.2023.107655

33. Namiki M, Ueda M, Todoroki A, Hirano Y, Matsuzaki R. 3D printing of continuous fiber reinforced plastic. *International SAMPE Technical Conference*. Published online 2014.

34. Chabaud G, Castro M, Denoual C, Le Duigou A. Hygromechanical properties of 3D printed continuous carbon and glass fibre reinforced polyamide composite for outdoor structural applications. *Addit Manuf*. 2019;26:94-105. doi:10.1016/j.addma.2019.01.005

35. Van Der Klift F, Koga Y, Todoroki A, Ueda M, Hirano Y, Matsuzaki R. 3D Printing of Continuous Carbon Fibre Reinforced Thermo-Plastic (CFRTP) Tensile Test Specimens. *Open Journal of Composite Materials*. 2016;06(01):18-27. doi:10.4236/ojcm.2016.61003

36. Peng Y, Wu Y, Wang K, Gao G, Ahzi S. Synergistic reinforcement of polyamide-based composites by combination of short and continuous carbon fibers via fused filament fabrication. *Compos Struct*. 2019;207:232-239. doi:10.1016/j.compstruct.2018.09.014

37. Kabir SMF, Mathur K, Seyam AFM. The Road to Improved Fiber-Reinforced 3D Printing Technology. *Technologies (Basel)*. 2020;8(4). doi:10.3390/technologies8040051

38. ASTM D6671/D6671M − 22. Standard Test Method for Mixed Mode I-Mode II Interlaminar Fracture Toughness of Unidirectional Fiber Reinforced Polymer Matrix Composites. In: *Annual Book of ASTM Standards*. Vol 15-03. American Society for Testing and Materials; 2022. doi:10.1520/D6671_D6671M-22

39. Pickering KL, Efendy MGA, Le TM. A review of recent developments in natural fibre composites and their mechanical performance. *Compos Part A Appl Sci Manuf*. 2016;83:98-112. doi:10.1016/j.compositesa.2015.08.038

40. Pai CC, Jeng RJ, Grossman SJ, Huang JC. Effects of moisture on thermal and mechanical properties of nylon-6,6. *Advances in Polymer Technology*. 1989;9(2):157-163. doi:https://doi.org/10.1002/adv.1989.060090206

41. Jia N, Fraenkel HA, Kagan VA. Effects of Moisture Conditioning Methods on Mechanical Properties of Injection Molded Nylon 6. *Journal of Reinforced Plastics and Composites*. 2004;23(7):729-737. doi:10.1177/0731684404030730

42. Paris AJ, Paris PC. Instantaneous evaluation of J and C. *Int J Fract*. 1988;38(1):R19-R21. doi:10.1007/BF00034281

43. Sarrado C. *Experimental Characterization and Numerical Simulation of Composite Adhesive Joints Using the Cohesive Zone Model Approach*. PhD thesis. Universitat de Girona; 2015.

44. Hashemi S, Kinloch AJ, Williams JG. The analysis of interlaminar fracture in uniaxial fiber-polymer composites. *Proceedings of the Royal Society of London Series A-Mathematical Physical and Engineering Sciences*. 1990;427(1872):173-199.

45. Kinloch AJ, Wang Y, Williams JG, Yayla P. The mixed-mode delamination of fiber composite-materials. *Compos Sci Technol*. 1993;47(3):225-237.

46. Santos JD, Guerrero JM, Blanco N, Fajardo JI, Paltán CA. Numerical and Experimental Analysis of the Mode I Interlaminar Fracture Toughness in Multidirectional 3D-Printed Thermoplastic Composites Reinforced with Continuous Carbon Fiber. *Polymers (Basel)*. 2023;15(10). doi:10.3390/polym15102403

47. Kabir SMF, Mathur K, Seyam AFM. A critical review on 3D printed continuous fiber-reinforced composites: History, mechanism, materials and properties. *Compos Struct*. 2020;232. doi:10.1016/j.compstruct.2019.111476

48. Oberlercher H, Heim R, Laux M, et al. Additive manufacturing of continuous carbon fiber reinforced polyamide 6: The effect of process parameters on the microstructure and mechanical properties. In: *Procedia Structural Integrity*. Vol 34. Elsevier B.V.; 2021:111-120. doi:10.1016/j.prostr.2021.12.017

49. Dang Z, Cao J, Pagani A, Zhang C. Fracture toughness determination and mechanism for mode-I interlaminar failure of 3D-printed carbon-Kevlar composites. *Composites Communications*. 2023;39. doi:10.1016/j.coco.2023.101532

50. Conroy M, Kinloch AJ, Williams JG, Ivankovic A. Mixed mode partitioning of beam-like geometries: A damage dependent solution. *Eng Fract Mech*. 2015;149(1):351-367. doi:10.1016/j.engfracmech.2015.06.061

51. Dillard DA, Singh HK, Pohlit DJ, Starbuck JM. Observations of decreased fracture toughness for mixed mode fracture testing of adhesively bonded joints. In: *Journal of Adhesion Science and Technology*. Vol 23. ; 2009:1515-1530. doi:10.1163/156856109X452701

52. DIN EN 2564:2019-08. *Aerospace Series - Carbon Fibre Laminates - Determination of the Fibre, Resin and Void Contents*. European Standard; 2018.

53. Yavas D, Zhang Z, Liu Q, Wu D. Interlaminar shear behavior of continuous and short carbon fiber reinforced polymer composites fabricated by additive manufacturing. *Compos B Eng*. 2021;204:108460. doi:10.1016/j.compositesb.2020.108460

54. He Q, Wang H, Fu K, Ye L. 3D printed continuous CF/PA6 composites: Effect of microscopic voids on mechanical performance. *Compos Sci Technol*. 2020;191(December 2018):108077. doi:10.1016/j.compscitech.2020.108077

55. Saeed K, McIlhagger A, Harkin-Jones E, Kelly J, Archer E. Predication of the in-plane mechanical properties of continuous carbon fibre reinforced 3D printed polymer composites using classical laminated-plate theory. *Compos Struct*. 2021;259. doi:10.1016/j.compstruct.2020.113226

56. Saeed K, McIlhagger A, Harkin-Jones E, et al. Characterization of continuous carbon fibre reinforced 3D printed polymer composites with varying fibre volume fractions. *Compos Struct*. 2022;282. doi:10.1016/j.compstruct.2021.115033

57. Iragi M. *Caracterización y Modelización Del Comportamiento Mecánico de Materiales Compuestos de Fibra Continua Con Orientaciones No-Convencionales Fabricados Mediante Impresión 3D*. PhD Thesis. Mondragon Unibertsitatea; 2022.